# We are IntechOpen, the world's leading publisher of Open Access books Built by scientists, for scientists

**6,900**
Open access books available

**186,000**
International authors and editors

**200M**
Downloads

Our authors are among the

**154**
Countries delivered to

**TOP 1%**
most cited scientists

**12.2%**
Contributors from top 500 universities

CLARIVATE ANALYTICS
**BOOK CITATION INDEX**
INDEXED

**WEB OF SCIENCE**™

Selection of our books indexed in the Book Citation Index
in Web of Science™ Core Collection (BKCI)

## Interested in publishing with us?
Contact book.department@intechopen.com

Numbers displayed above are based on latest data collected.
For more information visit www.intechopen.com

# Shape Control of Highly Crystallized Titania Nanorods for Dye-Sensitized Solar Cells Based on Formation Mechanism

Motonari Adachi[1,4], Katsuya Yoshida[2], Takehiro Kurata[2],
Jun Adachi[3], Katsumi Tsuchiya[2], Yasushige Mori[2] and Fumio Uchida[4]
*[1]Research Center of Interfacial Phenomena, Faculty of Science and Engineering,*
*Doshisha University, 1-3 Miyakodani, Tatara, Kyotanabe,*
*[2]Department of Chemical Engineering and Materials Science,*
*Doshisha University, 1-3 Miyakodani, Tatara, Kyotanabe,*
*[3]National Instituite of Biomedical Innovation, 7-6-8 Asagi Saito, Ibaraki,*
*[4]Fuji Chemical Co., Ltd., 1-35-1 Deyashikinishi-machi, Hirakata,*
*Japan*

## 1. Introduction

Utilization of solar energy - the part transmitted to the earth in the form of light- relies on how effectively it can be converted into the form of electricity. In this regard, dye-sensitized solar cells have attracted recent attention as they are expected to offer the possibility of inexpensive yet efficient solar energy conversion. The performance of dye-sensitized solar cells depends critically on a constituent nanocrystalline wide-band-gap semiconductor (usually titania, $TiO_2$, nanoparticles) on which a dye is adsorbed. The electrical and optical properties of such nanoparticles are often dependent on their morphology and crystallinity in addition to size, and hence, it is essential to be able to control the particle size, shape, their distributions and crystallinity (Empedocles et al., 1999; Nirmal & Brus, 1999; Manna et al., 2000), which requires an in-depth understanding of the mechanisms of nucleation and growth as well as such processes as aggregation and coarsening.

Among the unique properties exhibited by nanomaterials, the movement of electrons and holes in semiconductor materials is dominated mainly by the well-known quantum confinement, and the transport properties related to phonons and photons are largely affected by the size, geometry, and crystallinity of the materials (Alivisatos, 1996a, 1996b; Murray et al., 2000; Burda et al., 2005). Up to now, various ideas for morphological control were introduced (Masuda & Fukuda, 1995; Masuda et al., 1997; Lakshmi et al., 1997a, 1997b; Penn & Banfield, 1998; Banfield et al., 2000; Peng et al., 2000; Puntes et al., 2001; Pacholski et al., 2002; Tang et al., 2002, 2004; Peng, 2003; Scher et al., 2003; Yu et al., 2003; Cao, 2004; Cheng et al., 2004; Cui et al., 2004; Garcia & Tello, 2004; Liu et al., 2004; Pei et al., 2004; Reiss et al., 2004; Song & Zhang, 2004; Wu et al., 2004; Yang et al., 2004; Zhang et al., 2004) based on: (1) a mixture of surfactants used to bind them selectively to the crystallographic faces for CdS (Scher et al., 2003), (2) monomer concentration and ligand effects for CdSe (Peng et al., 2000), (3) growth rate by controlling heating rate for $CoFe_2O_4$ (Song & Zhang, 2004), (4)

biological routes in peptide sequence for FePt (Reiss et al., 2004), (5) controlled removal of protecting organic stabilizer for CdTe (Yu et al., 2003; Tang et al., 2002, 2004), (6) anodic alumina used as a template (Masuda & Fukuda, 1995; Masuda et al., 1997), and (7) the "oriented attachment" mechanism for nanoparticles (Penn & Banfield, 1998; Banfield et al., 2000). A number of methods have been developed to control the shape of nanocrystals on the basis of these ideas.

Titanium dioxide has a great potential in alleviating the energy crisis through effective utilization of solar energy with photovoltaics and water splitting devices, and is believed to be the most promising material for the electrode of dye-sensitized solar cells (Fujishima & Honda, 1972; Fujishima et al., 2000; Hagfeldt & Grätzel, 2000; Grätzel, 2000, 2001, 2004, 2005; Nazeeruddin et al., 2005). To further pursue this potential in terms of its morphology in dispersion, we have synthesized highly crystallized nanoscale "one-dimensional" titania materials such as titania nanowires having network structure (Adachi et al., 2004) and titania nanorods (Jiu et al., 2006), which were confirmed to provide highly efficient dye-sensitized solar cells (Adachi et al., 2007, 2008; Kurata et al., 2010).

Extremely high crystalline features of nanorods can be perceived in the images of high-resolution transmission electron microscopy (Yoshida et al., 2008; Kurata et al., 2010) as shown in Fig. 1. A highly magnified, high-resolution transmission electron microscopy image (Fig. 1b) demonstrates a well-regulated alignment of titanium atoms in crystalline anatase structure with essentially no lattice defects. The $TiO_2$ anatase (101) face, (-101) face, and (001) face are clearly observed; a specific feature definitely captured and to be noted is that the nanorod edge is sharply demarcated by the kinks consisting of (101) and (-101) planes. Such bare anatase crystal with atomic alignment - anatase $TiO_2$ crystals not covered with amorphous or additional phases around the edge or rim - is extremely important, when used as the materials for the electrodes, to achieve high performance for electrons transport and dye adsorption in the dye-sensitized solar cells. The longitudinal direction of the nanorod is along the $c$-direction, and the lattice spacing of 0.95 nm for the (001) plane and that of 0.35 nm for the {101} plane agree quite well with the corresponding values recorded in JCPDS. Such visual evidence strongly supports that the electron transport rate in the titania nanorods is expected to be very rapid, bringing highly efficient dye-sensitized solar cells through the use of the titania nanorods as the materials for the electrodes.

So far we have attained the power conversion efficiency ranging from 8.52% (Kurata et al., 2010) to 8.93% (Yoshida et al., 2008) using these nanorods as the electrode of dye-sensitized solar cells. In order to realize further improvement in conversion efficiency, we need to investigate the ways to control the shape as well as size of these nanorods by maintaining the extremely high crystalline feature of the nanorods. To accomplish the proper control of size and shape of nanorods, we examined the formation processes of nanorods under the most suitable condition for making nanorods, which is called "standard condition" hereafter, the results of which were detailed in a published work (Kurata et al., 2010).

In this chapter we first present the formation processes of titania nanorods under the standard condition in reasonable depth (Kurata et al., 2010). We then present the effects of both the concentrations of reactants, especially ethylenediamine, and the temperature-change strategy on the formation processes of nanorods. Based on all these findings, shape and size control of highly crystallized titania nanorods was proposed and carried out, leading to high-aspect-ratio, longer titania nanorods with highly crystallized state being successfully synthesized. We finally present that high dispersion of titania nanorods having highly crystallized state can be attained with the help of acetylacetone.
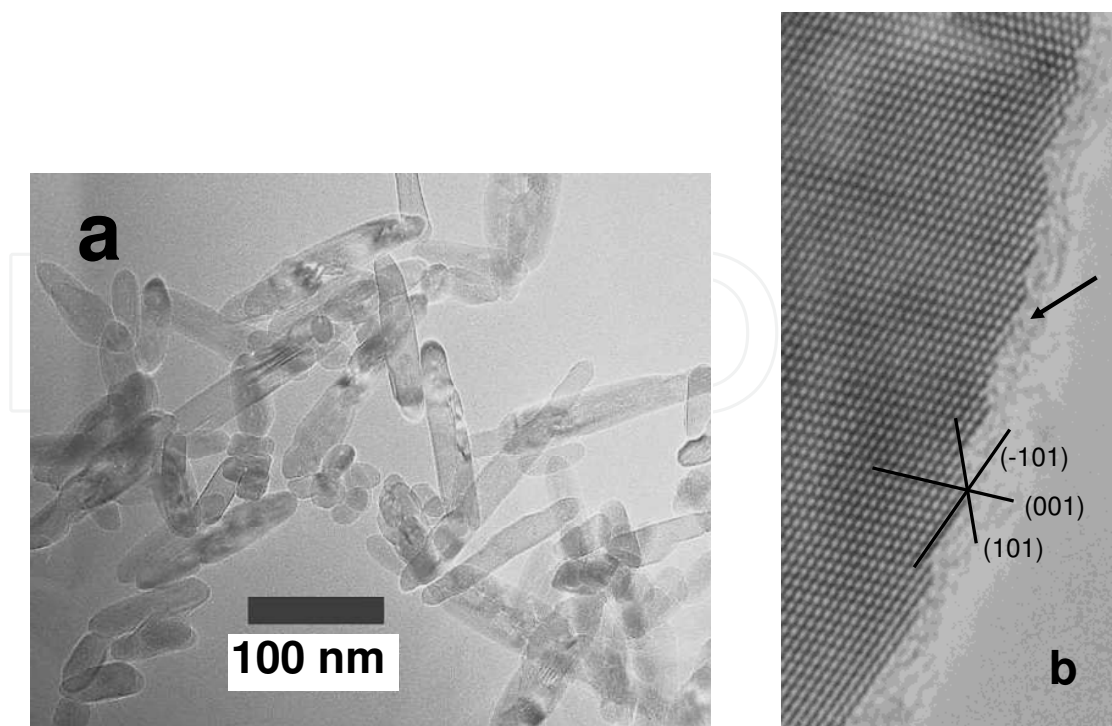
Fig. 1. Transmission electron microscopy images of highly crystallized titania nanorods covered with dye: (a) low-magnification image of titania nanorods, and (b) high-resolution image near the edge of a titania nanorod with dye coverage indicated by the arrow.

## 2. Experimental

The experimental procedure under the standard condition has been described in detail in our previous papers (Jiu et al., 2006; Kurata et al., 2010). Here, we summarize the essential part of the standard procedure and describe the modifications made on it. First, a 10-wt% aqueous solution of blockcopolymer F127 [(PEO)$_{106}$-(PPO)$_{70}$-(PEO)$_{106}$] was prepared using deionized pure water (Millipore Milli-Q). Cetyltrimethylammonium bromide was dissolved in the F127 solution at 308 K with a fixed concentration of cetyltrimethylammonium bromide, 0.055 M. In some modified cases the synthesis was carried out under no cetyltrimethylammonium bromide conditions. Ethylenediamine was added as a basic catalyst and also as a shape director (Sugimoto et al., 2003). The concentration of ethylenediamine was 0.25 M in the standard condition; in the modified conditions, the ethylenediamine concentration was varied from 0 to 0.5 M in order to examine its effects. After a transparent solution was obtained, tetraisopropyl orthotitanate (0.25 M) was added into the solution with stirring. This solution was stirred for half a day in the standard condition. The solution including white precipitates obtained by hydrolysis and condensation reactions of tetraisopropyl orthotitanate was then transferred into a Teflon autoclave sealed with a crust made of stainless steel, and reacted at 433 K for a desired period.

In the modified cases with temperature strategy, the reaction temperature was reduced during the preparation from 433 to 413 K to investigate its effects on the reaction mechanism. When acetylacetone was used to modify tetraisopropyl orthotitanate by binding acetylacetone to Ti atoms of tetraisopropyl orthotitanate, the transparent solutions were obtained after one-week stirring before hydrothermal reaction. The reaction product

obtained under the hydrothermal condition at a desired time was washed by isopropyl alcohol and deionized pure water, followed by separating the reaction product by centrifugation (Kokusan H-40F). After the washing, the obtained sample was dried in vacuum for 24 h (EYELA Vacuum Oven VOS-450-SD). To gain additional insight into the underlying mechanism for the transition from amorphous-like structure to titania anatase crystalline structure in the early stage of the reaction, changes in shape and crystalline structure of reaction products upon calcination at 723 K for 2 h were observed and measured.

## 3. Results and discussion

### 3.1 Formation processes under standard condition

First of all, the formation processes under the standard condition are described prior to comparing the experimental results and discussing the effects of various modifications on those under the modified conditions. Typical transmission electron microscopy images of reaction products at 0.5, 2, 3.5, 4, 6, and 24 h under the standard condition (Kurata et al., 2010) are shown in Fig. 2. At 0.5 h, only a film-like structure was observed. At 2 h, the shape of reaction products was still mostly film-like, while some deep-black wedge-shaped structure partly appeared. At 3.5 h, the main structure was still film-like, with uneven light and dark patches recognized. At 4 h, however, only rod-shaped products were observable, signifying that the film-like shape with amorphous-like structure changed to nanorod-shaped titania in a time interval between 3.5 and 4 h. After 6 h, only nanorod shape was observed. The morphology was observed to change very slowly with time after 6 h.
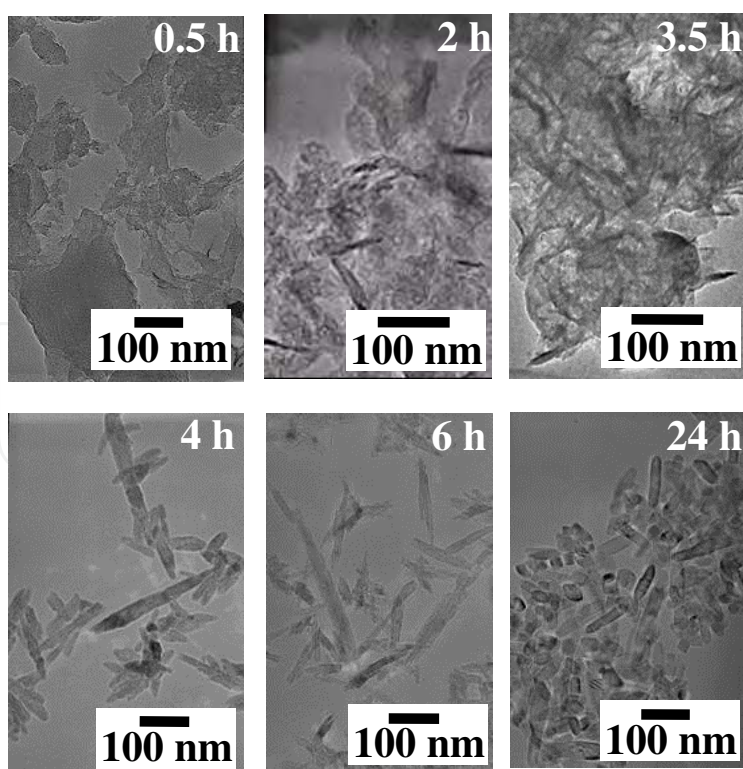


Fig. 2. Transmission electron microscopy images of reaction products at 0.5, 2, 3.5, 4, 6, and 24 h under standard condition (Kutata et al., 2010).
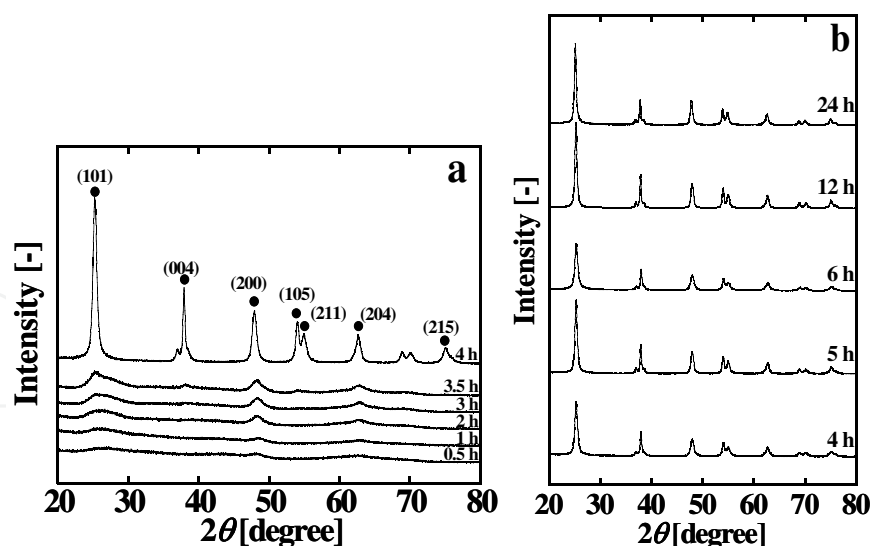
Fig. 3. Variation in X-ray diffraction spectra of reaction products: (a) from 0.5 to 4 h, (b) from 4 to 24 h.

Fig. 3 shows the variation in X-ray diffraction spectra (a) from 0.5 to 4 h and (b) from 4 to 24 h under the standard condition (Kurata et al., 2010), i.e., 0.25-M tetraisopropyl orthotitanate, 10-wt% F127, 0.055-M cetyltrimethylammonium bromide, 0.25-M ethylenediamine, and at 433 K. In the initial stage of reaction, X-ray diffraction spectra showed almost no clear peak, indicating the $TiO_2$ formed was amorphous. From 2 to 3.5 h, tiny and broad anatase peaks appeared, but the main structure of titania was still amorphous-like. During 3.5 to 4 h interval, a drastic change in the X-ray diffraction spectrum was detected, signifying the evolution from amorphous-like to clear anatase crystalline structure. From 4 to 24 h, X-ray diffraction spectra showed no appreciable changes.

In order to investigate the underlying process for the transition from amorphous-like structure to titania anatase crystalline structure in the early stage of the reaction, variations in shape and crystalline structure of reaction products upon calcination at 723 K for 2 h were utilized by Kurata et al. (2010). Fig. 4 shows the structural change from amorphous to anatase phase at 0.5 h after calcination, and the amorphous-like structure at 2 and 3.5 h also changing to anatase phase. At 4 h, the anatase crystalline structure was already formed before calcination. After 6 h, the X-ray diffraction patterns obtained before calcination almost completely coincided with those after calcination, indicating that crystalline structure before calcination did not change upon calcination owing to the highly crystallized state already achieved prior to calcination.

Transmission electron microscopy images of reaction products at reaction times of 0.5, 2, 3.5, 4, 6, and 24 h after calcination at 723 K for 2 h (Kurata et al., 2010) are shown in Fig. 5. Titania anatase nanoparticles with diameter around 10 nm were identifiable for the reaction products obtained at 0.5 h upon the calcination. While the product obtained at 1 h also changed to nanoparticles, the product obtained at 2 h changed to a mixture of nanoparticles and nanorods on the calcination. Similarly, a mixture of nanoparticles and nanorods were obtained for the product of 3.5 h upon the calcination. The fraction of rods at 3.5 h increased in comparison with that at 2 h. The nanorods formation could thus be claimed to be attributed to the growth of nuclei with anatase-like structure on the calcination. X-ray diffraction spectra before the calcination at 2 and 3.5 h were quite different from those of highly crystallized titania anatase at 6 and 24 h.
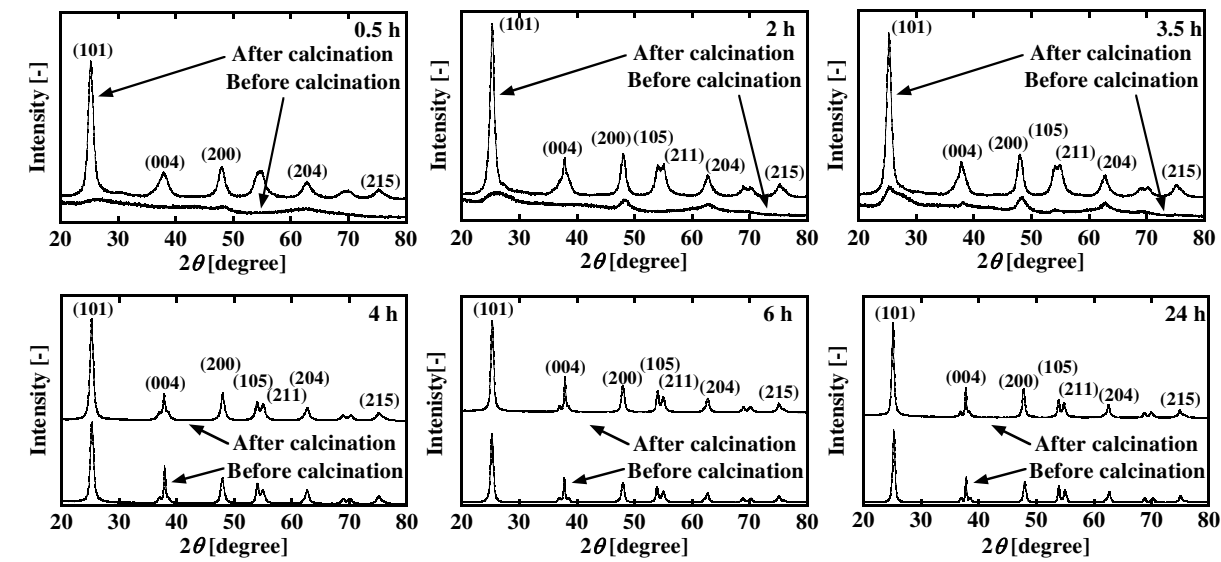
Fig. 4. Variation in X-ray diffraction patterns of reaction products upon calcination at 723 K for 2 h for the samples obtained at reaction times of 0.5, 2, 3.5, 4, 6, and 24 h.

The peak at 48.3 deg corresponding to (200) plane ($2\theta$ = 48.1 deg) in anatase phase was clearly observable and larger than those at 37.7 and 63 deg corresponding to (004) and (204) planes. Furthermore, no peak is observable at 38.6 deg, which corresponds to characteristic peak of (11) plane of Lepidocrocite (two-dimensional titania crystal). Therefore, the crystalline structure generated from film-like amorphous phase is inferred to be very thin two-dimensional anatase crystal.
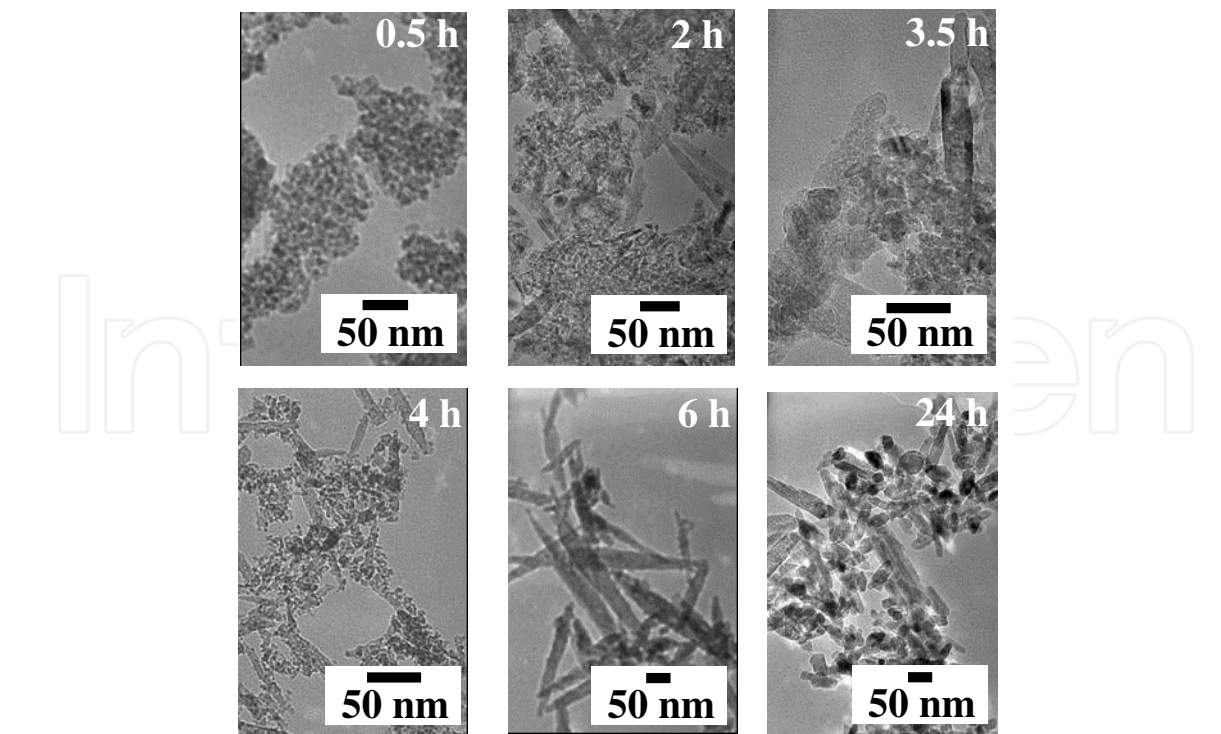


Fig. 5. Transmission electron microscopy images of reaction products obtained at 0.5, 2, 3.5, 4, 6, and 24 h after calcination at 723 K for 2 h.

The intensity ratio of (004) peak to (200) peak in X-ray diffraction spectra is shown in Fig. 6 as a function of the reaction time before and after calcination (Kurata et al., 2010). The almost zero ratio was obtained from 0.5 to 2 h in the absence of calcination, indicating that ordering of amorphous titania from random connection to crystal, evidenced partly in Fig. 2 and 3, occurred only in the film with no growth in the $c$-axis. The ratio, then, had increased progressively up to 0.38 at 3.5 h revealing slight growth in the $c$-axis, until the ratio attained a maximum rate of increase between 3.5 and 4 h duration, corresponding to the drastic change in the shape and crystalline structure of reaction products. Such an overwhelming increase in the intensity ratio (004)/(200) indicates that the phase transition from amorphous-like phase to anatase phase can bring about significant growth in the $c$-axis. The highest value was obtained at 4 h and slightly decreased with time, asymptotically approaching a constant of ~1.2 after 6 h. After calcination, the ratio gradually increased from 0.5 up to 6 h, and then reached a constant value, which was identical to the value obtained before calcination. These two distinctive trends shown in Fig. 6 signify that the crystalline structure of nanorods did not change on calcination, maintaining the intensity ratio at the same asymptotic level (~1.2) before and after calcination.
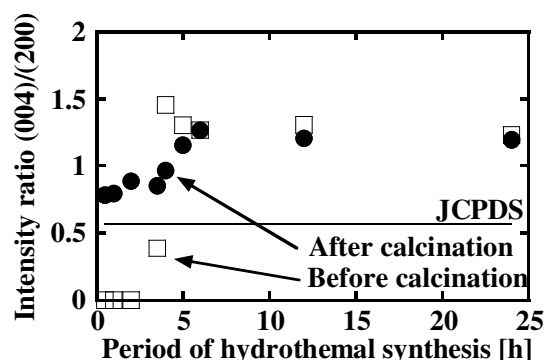


Fig. 6. Intensity ratio of (004) peak to (200) peak in X-ray diffraction spectra with reaction time under conditions before and after calcination.

## 3.2 Effects of ethylenediamine concentration and temperature change on the formation processes of nanorods

We investigated the effects of both ethylenediamine concentration and temperature change on the formation processes of nanorods. In particular, their mechanistic contributions to size and shape control of highly crystallized titania nanorods were inferred, together with the results of formation processes under standard condition mentioned above.
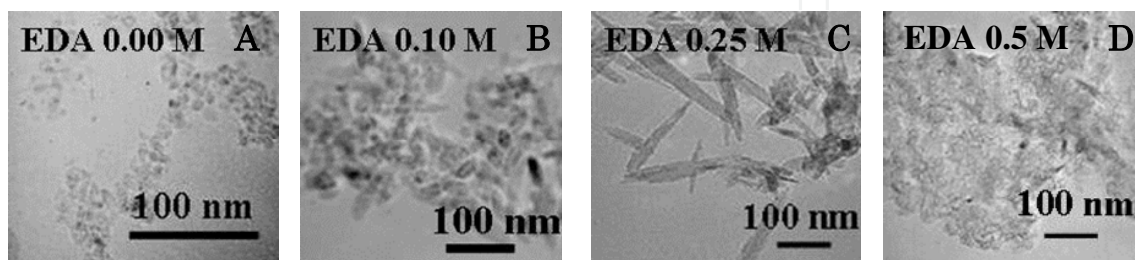


Fig. 7. Transmission electron microscopy images of reaction products synthesized at different ethylenediamine concentrations by hydrothermal method. Reaction conditions: 433 K, 6 h. "EDA" designates ethylenediamine.

Fig. 7 shows the effects of ethylenediamine concentration on the morphology of reaction products at 433 K for 6 h. When the ethylenediamine concentration was 0, titania particles with aspect ratio of roughly unity were formed. As the concentration was changed from 0 to 0.1 M, the morphology of titania shifted from particulate to a mixture of particles and rods. As the concentration reached 0.25 M (i.e., the value used under the standard condition, and thus as expected), only nanorods were observed to form, while at an ethylenediamine concentration as high as 0.5 M the observed products appeared to be unexpectedly film-like titanate. The corresponding X-ray diffraction spectra for the given series of samples are shown in Fig. 8. When the ethylenediamine concentration was 0 M, typical anatase peaks were obtained where (004) peak has a lower height than (200) peak, matching the spherical shape observed in Fig. 7A. When the ethylenediamine concentration was 0.25 M, a clear anatase spectrum was observed with higher (004) peak in comparison to (200) peak, signifying the formation of titania nanorods. For 0.1-M ethylenediamine concentration an intermediate spectrum between those of 0 and 0.25 M was observed due to the formation of particle-rod mixture as discussed above (see Fig. 7B). When the concentration became 0.5 M, a weak amorphous-like spectrum was obtained, corresponding to the observation of film-like structure in Fig. 7D. All these results signify that there should exist an optimum ethylenediamine concentration for controlling the rate of formation of titania nanorods at ≈ 0.25 M, above which - specifically at as high as 0.5 M - the reaction rate tends to slow down; that is, the morphological transition would be delayed. Such inference could be made by referring the morphology transformation as depicted in Fig. 2 under the standard condition with 0.25-M ethylenediamine.
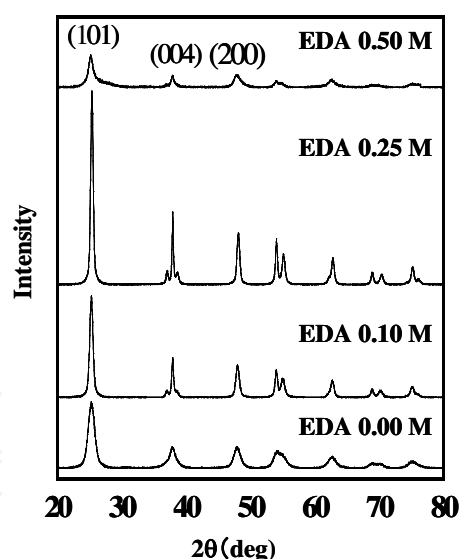
Fig. 8. X-ray diffraction spectra of the same samples shown in Fig. 7.

To further investigate the formation processes of titania nanorods at this high ethylenediamine concentration of 0.5 M, we carried out a series of experiments for evaluating the time course of the formation processes; the results are shown in Fig. 9. Film-like structure was observed up to 6 h as stated above; after 8 h, however, only rod shape was identifiable, signifying that the transformation from the amorphous film-like structure to the anatase titania nanorods has been almost completed by this time. Fig. 10 shows transmission electron microscopy and high-resolution transmission electron microscopy images of the

reaction product obtained at 45 h. Ordered alignment of titania atoms in anatase structure can be clearly perceived, indicating the formation of highly crystallized titania anatase nanorods.
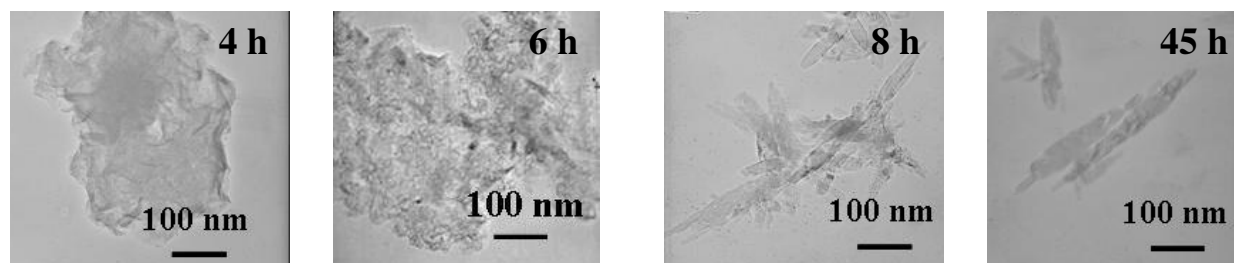


Fig. 9. Transmission electron microscopy images of reaction products obtained at different reaction times for 0.5-M ethylenediamine concentration. The rest of reaction conditions are the same as in the standard condition.

The effect of temperature change/reduction was examined by obtaining the time course of the formation processes at 413 K based on scanning electron microscopy images and X-ray diffraction measurements; the results are shown in Figs. 11 and 12, respectively. As shown in Fig. 11, the film-like structure was still observed at even 36 h. The X-ray diffraction spectrum obtained at 36 h shows no significant peaks, i.e., amorphous-like phase formation, which was observed under the standard condition at only up to 3.5 h (see Fig. 3a). Therefore, the reaction rate at 413 K became significantly slower. From scanning electron microscopy images, coexistence of titania nanorods and film was observed until 56 h, which was never recognized at the standard reaction temperature 433 K. It was after 64 h that only titania nanorods were finally observed. The scanning electron microscopy image obtained at 64 h shows a wide distribution in length of nanorods from roughly 10 to 600 nm, implying that nucleation and growth of nanorods would proceed concurrently because of the slow reaction rate at 413 K. The X-ray diffraction spectrum at 48 h, on the other hand, shows anatase peaks, though each peak height is not high. The peak height increases gradually with time up to 64 h. This observation suggests again the coexistence of amorphous-like films and titania nanorods. The peak height becomes higher with an increase in the fraction of titania nanorods up to 64 h.
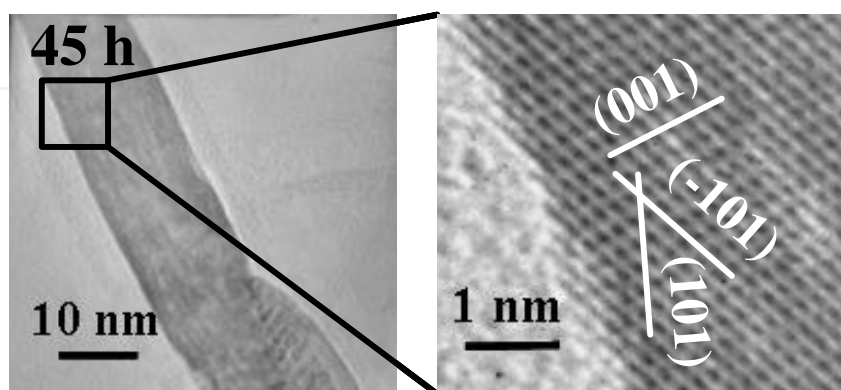


Fig. 10. Transmission electron microscopy and high-resolution transmission electron microscopy images of reaction product obtained at 45 h under 0.5-M ethylenediamine.
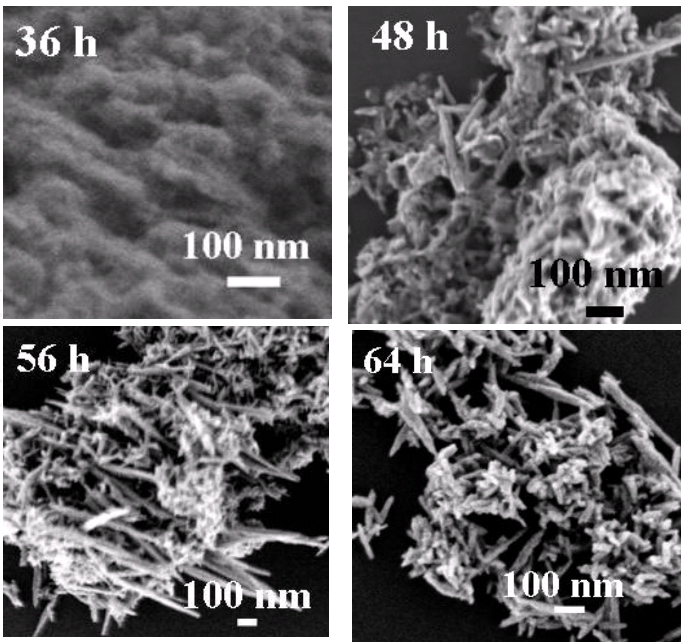
Fig. 11. Scanning electron microscopy images of reaction products obtained under the condition of 413 K at various times.



Fig. 12. X-ray diffraction patterns of the same reaction products of Fig. 11.

The observations and measurements made on temperature change described above are summarized in Fig. 13. At 413 K, the reaction is slow, resulting in concurrence of nucleation and growth of nanorods. At 433 K, on the other hand, the reaction occurs rapidly, resulting in 1) the prevalence of nucleation almost exclusively in the amorphous phase in the early reaction stage, 2) a drastic change from amorphous phase to crystalline titania anatase nanorods, and 3) no concurrence of nucleation and growth of nanorods. These findings should give some hints for the strategy for size and shape control.

```
┌──────────┐   Slow reaction rate   ┌────────────────────────┐
│ At 140℃ │ ─────────────────────→ │ Concurrence of nucleation │
└──────────┘                        │ and growth of nanorods │
                                    └────────────────────────┘

┌──────────┐   Fast reaction rate   ┌────────────────────────┐
│ At 160℃ │ ─────────────────────→ │ Nucleation occurring only │
└──────────┘                        │ in amorphous phase     │
                                    ├────────────────────────┤
                                    │ Drastic change in      │
                                    │ structure from amorphous │
                                    │ phase to crystalline titania │
                                    │ nanorods               │
                                    ├────────────────────────┤
                                    │ No concurrence of      │
                                    │ nucleation and growth of │
                                    │ nanorods               │
                                    └────────────────────────┘
```
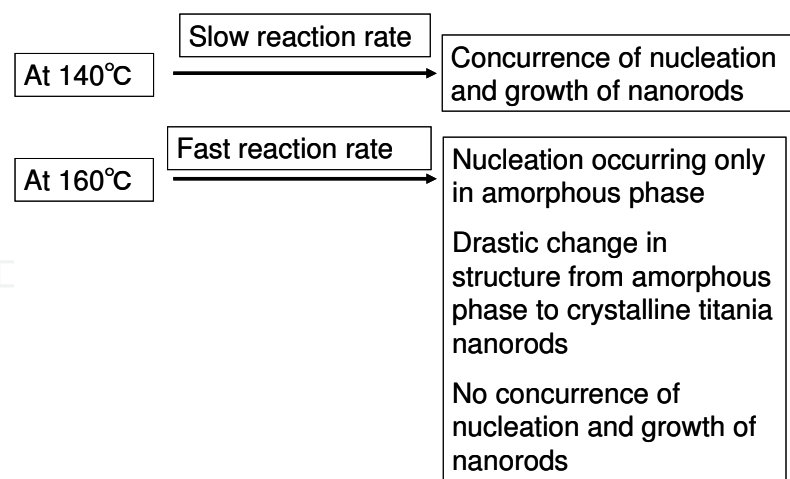
Fig. 13. Effects of reaction temperature on characteristics of formation processes at 413 K and 433 K.

### 3.3 Strategy for shape and size control of highly crystallized titania nanorods

The proposed strategy is given in Fig. 14. Nuclei are to be generated at a higher temperature 433 K in the early stage of reaction. These nuclei formed coincidently are to be reacted at a reduced temperature 413 K under hydrothermal conditions without further nucleation. Then, growth of rather uniform-sized and shaped nanorods is expected, in the aid of high concentration of ethylenediamine in effectively reducing their nucleation rate. In addition, we can also use the effectiveness of acetylacetone in obtaining good dispersion of nanorods (to be discussed later).

```
                    ┌──────────────────────────┐
                    │ Nuclei to be formed at 160℃ │
                    │ in early stage of reaction │
                    └──────────────────────────┘
┌──────────────┐                │
│ Hydrothermal │                │
│ reaction at 140 ℃ │            ↓
└──────────────┘    ┌──────────────────────────┐
                    │ Growth of uniform size   │
                    │ nanorods without nucleation │
                    └──────────────────────────┘
                       ↗                    ↖
┌──────────────────┐          ┌──────────────────────────┐
│ Effectiveness of │          │ Effectiveness of acetylacetone │
│ high concentration │        │ in obtaining good dispersion │
│ of ethylenediamine │        └──────────────────────────┘
│ in reducing       │
│ nucleation rate   │
└──────────────────┘
```
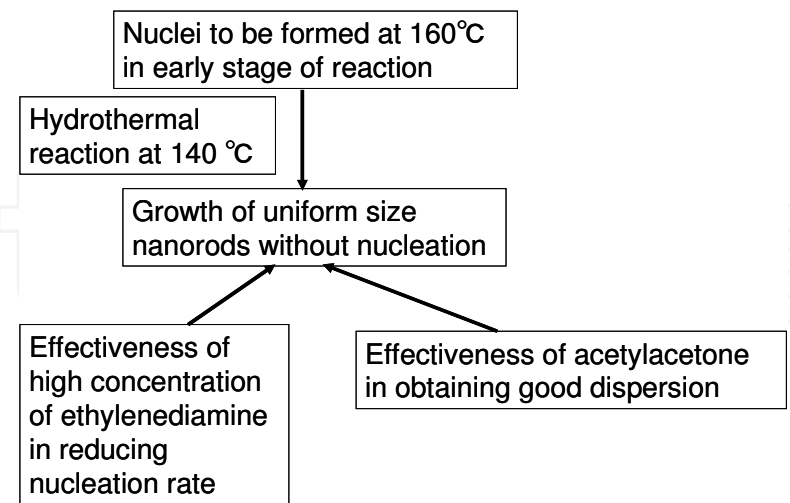
Fig. 14. Strategy for size and shape control of titania nanorods.

The specific preparation procedures are as follows. The even formation of nuclei was attempted at 433 K under the standard condition via the hydrothermal reaction for 2 h before being cooled down to room temperature. Ethylenediamine was then added to have

its concentration be 0.5 M for selectively reducing nucleation rate. Formation reaction with these precursory nuclei was successively carried out at 413 K under the hydrothermal condition for 52 h; the reaction conditions are in the following: 0.25-M tetraisopropyl orthotitanate, 10-wt% F127, 0.055-M cetyltrimethylammonium bromide and 0.5-M ethylenediamine. A transmission electron microscopy image of thus obtained nanorods is shown in Fig. 15. Over 800-nm long, high-aspect-ratio nanorods were indeed obtained. In comparison to the nanorods images for 433 K at 24 h shown in Fig. 2 and those for 413 K at 64 h in Fig. 11, the nanorods obtained based on the proposed shape-control strategy were certainly improved in terms of morphological uniformity, despite the presence of some shorter nanorods, which stems from the not completely avoidable occurrence of nucleation during the formation reaction.
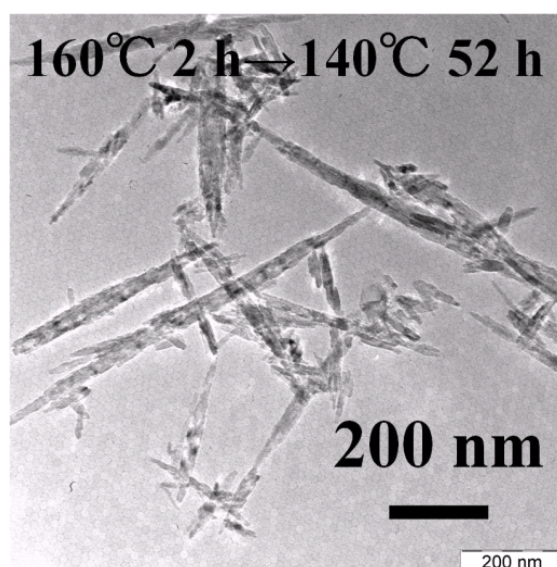


Fig. 15. Transmission elecron microscopy image of shape-controlled nanorods prepared based on the strategy given in Fig. 14.

### 3.4 Highly dispersed titania nanorods obtained with the help of acetylacetone

The effect of addition of acetylacetone was examined separately. In the experiments the same moles of acetylacetone and tetraisopropyl orthotitanate were mixed with each other to make a 1:1 complex. The complex was added to an aqueous solution of 10-wt% F127 containing 0.3-0.5 M ethylenediamine but no cetyltrimethylammonium bromide. The solution was stirred for one week at room temperature. The solution became transparent after 1-week stirring, which was never observed in the absence of acetylacetone. Adding acetylacetone thus must have a critical effect on particle dispersion. An example of nanorods thus obtained is shown in Fig. 16 (top) under the condition of 0.3-M ethylenediamine. Very good dispersion of titania nanorods was attained, and highly crystallized state is obvious as demonstrated in the high-resolution image in Fig. 16 (bottom). Since acetylacetone is known to adsorb on the surface of titania anatase crystal (Connor et al., 1995), adsorbed acetylacetone molecules could prevent aggregation of titania nanorods, resulting in such good dispersion. Also, since acetylacetone is expected to affect the formation mechanism, utilization of acetylacetone might improve the shape-control scheme of nanorods.
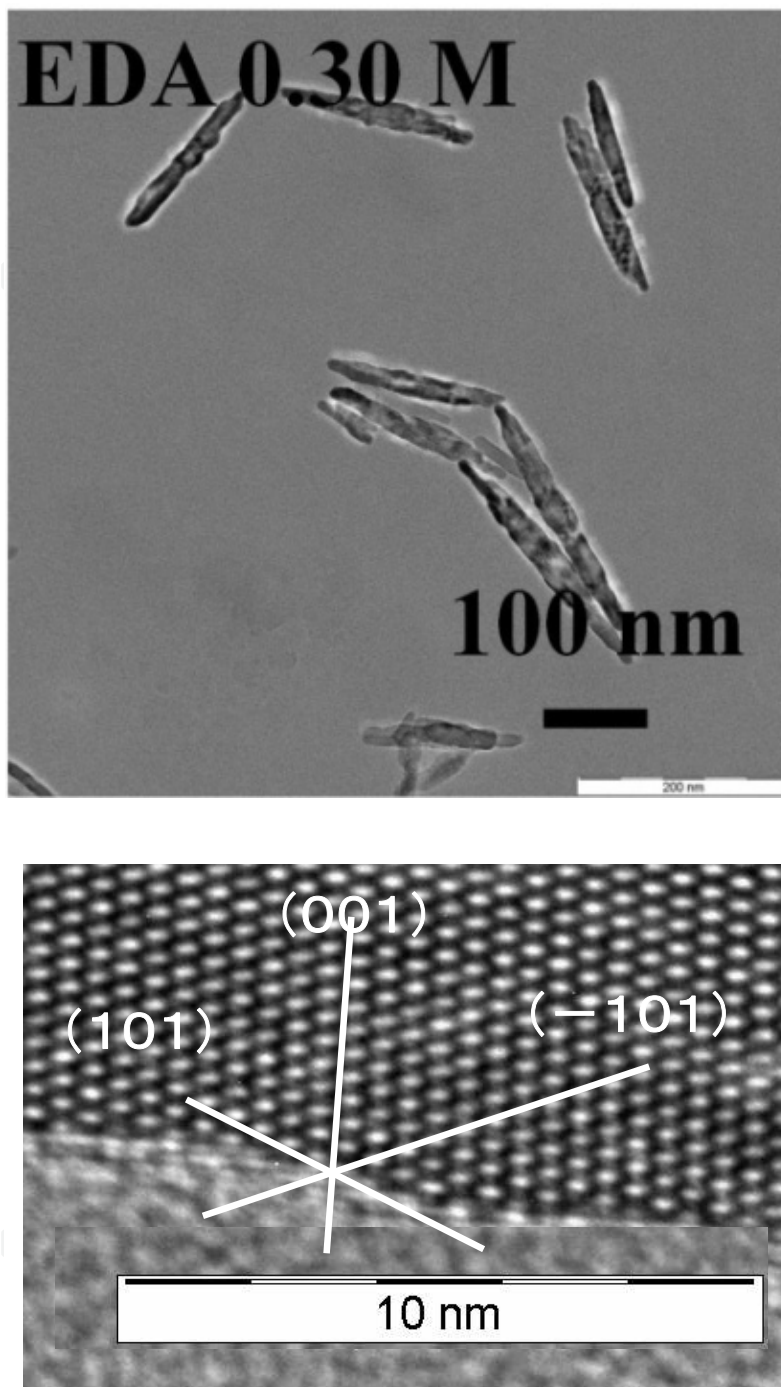
Fig. 16. Highly dispersed titania nanorods obtained with the help of acetylacetone (top) and highly crystallized feature of the nanorods demonstrated by high-resolution transmission electron microscpy image (bottom).

### 3.5 Application for dye-sensitized solar cells

The application of highly crystallized titania nanorods for making dye-sensitized solar cells was already reported (Yoshida et al., 2008; Kurata et al., 2010). A titania electrode made of titania nanorods was successfully fabricated as follows. The complex electrodes were

prepared by the repetitive coating-calcining process: 3 layers of titania nanoparticles (Jiu et al., 2004, 2007) were first coated on FTO conducting glass, followed by 7 layers of mixed gel composed of titania nanorods and P-25. High light-to-electricity conversion efficiencies of 8.52 to 8.93% were achieved as exemplified in Fig. 17. We are now trying to get much higher power conversion efficiency by utilizing the shape-controlled, highly crystallized titania nanorods with high dispersion as a titania electrode of dye-sensitized solar cells.



Fig. 17. I-V curve for complex dye-sensitized solar cell electrode consisting of highly crystallized titania nanorods, P-25, and titania nanoparticles.

## 4. Conclusions

The formation processes of highly crystallized titania nanorods were revealed in detail under 10-wt% F127, 0.25-M tetraisopropyl orthotitanate, 0.055-M cetyltrimethylammonium bromide, 0.25-M ethylenediamine, and 433 K (standard) conditions.

Strategy for shape and size control of highly crystallized titania nanorods was proposed through the findings obtained by examining the effects of both ethylenediamine concentration and temperature change on the formation processes of titania nanorods. Over 800-nm long and high-aspect-ratio, highly crystallized titania nanorods were successfully synthesized following the proposed strategy.

## 5. References

Adachi, M. Jiu, J. & Isoda, S. (2007). Synthesis of morphology-controlled titania nanocrystals and application for dye-sensitized solar cells. *Current Nanoscience*, 3, pp. 285-295

Adachi, M. Jiu, J. Isoda, S. Mori, Y. & Uchida, F. (2008). Self-assembled nanoscale architecture of $TiO_2$ and application for dye-sensitized solar cells. *Nanotechnology. Science and Applications*, 1, pp. 1-7

Adachi, M. Murata, Y. Takao, J. Jiu, J. Sakamoto, M. & Wang, F. (2004). Highly efficient dye-sensitized solar cells with titania thin film electrode composed of network structure of single-crystal-like $TiO_2$ nanowires made by "Oriented Attachment" mechanism. *J. Am. Chem. Soc.*, 126, pp. 14943-14949

Adachi, M. Sakamoto, M. Jiu, J. Ogata, Y. & Isoda, S. (2006). Determination of parameters of electron transport in dye-sensitized solar cells using electrochemical impedance spectroscopy. *J. Phys. Chem. B* 110, pp. 13872-13880

Alivisatos, A. P. (1996a). Semiconductor Clusters, Nanocrystals, and Quantum Dots. *Science*, 271, pp. 933-937

Alivisatos, A. P. (1996b). Perspectives on the physical chemistry of semiconductor nanocrystals. *J. Phys. Chem.*, 100, pp. 13226-13239

Banfield, J. F. Welch, S. A. Zhang, H. Ebert, T. T. & Penn, R. L. (2000). Aggregation-based crystal growth and microstructure development in natural iron oxyhydroxide biomineralization products. *Science*, 289, pp. 751-754

Burda, C. Chen, X. Narayanan, R. & El-Sayed, M. A. (2005). Chemistry and properties of nanocrystals of different shapes. *Chem. Rev.*, 105, pp. 1025-1102

Cao Y. C. (2004) Synthesis of square gadolinium-oxide nanoplates. *J. Am. Chem. Soc.*, 126, pp. 7456-7457

Cheng, B. Rusell, J. M. Shi, W. Zhang, L. & Samulski, E. T. (2004). Large-scale, solution-phase growth of single-crystalline $SnO_2$ nanorods. *J. Am. Chem. Soc.*, 126, pp. 5972-5973

Connor, P. A.. Dobson, K. D & McQuillan: A. J. (1995). New sol-gel attenuated total reflection infrared spectroscopic method for analysis of adsorption at metal oxide surface in aqueous solution. Chelation of TiO2, ZrO2, and Al2O3 surfaces by catechol, 8-quinolinol, and acetylacetopne. *Langmuir*, 11, pp. 4193-4195

Cui, Y. Bjork, M. T. Liddle, J. A. Sonnichsen, C. Boussert, B. & Alivisatos, A. P. (2004). Integration of colloidal nanocrystals into lithographically patterned devices. *Nano Lett.*, 4, pp. 1093-1098

Empedocles, S. A. Neuhauser, R. Shimizu, K. & Bawendi, M. G. (1999). Photoluminescence from single semiconductor nanostructures. *Adv. Mater.*, 11, pp. 1243-1256

Fabregat-Santiago, F. Bisquert, J. Palomares, E. Kuang, D. Zakeeruddin, S. M. & Grätzel, M. (2007). Correlation between photovoltaic performance and impedance spectroscopy of dye-sensitized solar cells based on ionic liquid: *J. Phys. Chem. C*, 111, pp. 6550-6560

Fujishima, A. & Honda, K. (1972). Electrochemical photolysis of water at a semiconductor electrode. *Nature*, 238, pp. 37-38

Fujishima, A. Rao, T. N. & Tryk, D. A. (2000). Titanium dioxide photocatalysis. *J. Photpchem. Photobio. C*, 1, pp. 1-21

Fukuda, K. Ebina, Y. Shibata, T. Aizawa, T. Nakai, I. & Sasaki, T. (2007) Unusual crystallization behaviors of anatase nanocrystallites from a molecularly thin titania
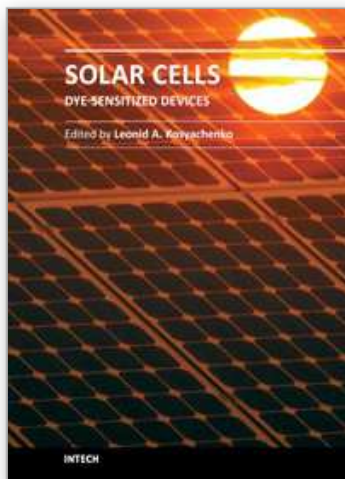
nanosheet and its stacked forms: Increase in nucleation temperature and oriented growth. *J. Am. Chem. Soc.*, 129, pp. 202-209.

Garcia, R. & Tello, R. (2004). Size and shape controlled growth of molecular nano-structures on silicon oxide templates. *Nano Lett.*, 4, pp. 1115-1119

Grätzel, M. (2000). Photovoltaic performance and long-term stability of dye-sensitized meosocopic solar cells. *C. R. Chemie.*, 9, pp. 578-583

Grätzel, M. (2001). Photoelectrochemical cells. *Nature*, 414, pp. 338-344

Grätzel, M. (2004). Conversion of sunlight to electric power by nanocrystalline dye-sensitized solar cells. *J. Photpchem. Photobio. A: Chemistry*, 164, pp. 3-14

Grätzel, M. (2005). Solar Energy Conversion by Dye-Sensitized Photovoltaic Cells. *Inorg. Chem.*, 44, pp. 6841-6851

Hagfeldt, A. & Grätzel, M. (2000). Molecular photovoltaics. *Acc. Chem. Res.*, 33, pp. 269-277

Jiu, J. Isoda, S. Adachi, M. & Wang, F. (2007). Preparation of TiO2 nanocrystalline with 3-5 nm and application for dye-sensitized solar cell. *J. Photochem. Photobio. A: Cemistry*, 189, pp. 314-321

Jiu, J. Isoda, S. Wang, F. & Adachi, M. (2006). Dye-sensitized solar cells based on a single-crystalline TiO2 nanorod film. *J. Phys. Chem. B*, 110, pp. 2087-2092

Jiu, J. Wang, F. Sakamoto, M. Takao, J. & Adachi, M. (2004). Preparation of nanocrystaline TiO₂ with mixed template and its application for dye-sensitized solar cells. *J. Electrochem. Soc.*, 151, pp. A1653-A1658

Kurata, T. Mori, Y. Isoda, S. Jiu, J. Tsuchiya, K. Uchida, F. & Adachi, M. (2010). Characterization and formation process of highly crystallized single crystalline TiO₂ nanorods for dye-sensitized solar cells. *Current Nanoscience*, 6, pp. 269-276

Lakshmi, B. B. Dorhout, P. K. & Martin, C. R. (1997a). Sol-gel template synthesis of semiconductor nanostructures. *Chem. Mater.*, 9, pp. 857-862

Lakshmi, B. B. Dorhout, P. K. & Martin, C. R. (1997b). Sol-gel template synthesis of semiconductor oxide micro- and nanostructures. *Chem. Mater.*, 9, pp. 2544-2550

Liu, C. Wu, X. Klemmer, T. Shukla, N. Yang, X. Weller, D. Roy, A. G. Tanase, M.& Laughlin, D. (2004). Polyol process synthesis of monodispersed fept nanoparticles. *J. Phys. Chem. B*, 108, pp. 6121-6123

Manna, L. Scher, E. C. & Alivisatos, A. P. (2000). Synthesis of soluble and processable rod-, arrow-, teardrop-, and tetrapod-shaped CdSe nanocrystals. *J. Am. Chem. Soc.*, 122, pp. 12700-12706

Masuda, H. & Fukuda, K. (1995). Ordered Metal nanohole arrays made by a two-step replication of honeycomb structures of anodic alumina. *Science.* 268, pp. 1466-1468

Masuda, H. Yamada, H. Satoh, M. Asoh, H. Nakao, M. & Tamamura, T. (1997) Highly ordered nanochannel-array architecture in anodic alumina. *Appl. Phys. Lett.*, 71, pp. 2770-2772

Murray, C. B. Kagan, C. R. & Bawendi, M. G. (2000). Synthesis and characterization of monodisperse nanocrystals and close-packed nanocryatal assemblies. *Annu. Rev. Mater. Sci.*, 30, pp. 545-610

Nazeeruddin, M. K. De Angelis, F. Fantacci, S. Selloni, A. Viscardi, G. Liska, P. Ito, S. Bessho, T. & Graetzel, M. (2005) Combined experimental and DFT-TDDFT computational

study of photoelectrochemical cell ruthenium sensitizers. *J. Am. Chem. Soc.*, 127, pp. 16835-16847

Nirmal, M. & Brus, L. (1999). Luminescence photophysics in semiconductor nanocrystals. *Acc. Chem. Res.*, 32, pp. 407-414

Pacholski, C. Kornowski, A. & Weller, H. (2002). Self-assembly of ZnO: From nanodots to nanorods. *Angew. Chem. Int. Ed.*,. 41, pp. 1188-1191

Pei, L. Mori, K. & Adachi, M. (2004). Formation process of two-dimensional networked gold nanowires by citrate reduction of AuCl$_4^-$ and the shape stabilization. *Langmuir*, 20, pp. 7837-7843

Peng, X. (2003) Mechanisms for the shape-control and shape-evolution of colloidal semiconductor nanocrystals. *Adv. Mater.*, 15, pp. 459-463

Peng, X. G. Manna, L. Yang, W. D. Wickham, J. Scher, E. Kadavanich, A. & Alivisatos, A. P. (2000). Shape control of CdSe nanocrystals. *Nature*, 404, pp. 59-61

Penn, R. L. & Banfield, J. F. (1998). Morphology development and crystal growth in nanocrystalline aggregates under hydrothermal conditions: insights from titania. *Science*, 281, pp. 969-971

Puntes, V. F. Krishnan, K. M. & Alivisatos, A. P. (2001). Colloidal nanocrystal shape and size control: The case of cobalt. *Science*, 291, pp. 2115-2117

Reiss, B. D. Mao, C. Solis, D. J. Ryan, K. S. Thomson, T. & Belcher. (2004). A. M. Biological routes to metal alloy ferromagnetic nanostructures. *Nano Lett.*, 4, pp. 1127-1132

Scher, E. C. Soc, R. Manna, L.& Alivisatos, A. P. (2003). Shape control and applications of nanocrystals. *Phil. Trans. R. Soc.* Lond. A, 361, pp. 241-257

Song, Q. & Zhang, Z. J. Shape control and associated magnetic properties of spinel cobalt ferrite nanocrystals, J. (2004). *Am. Chem. Soc.*, 126, pp. 6164-6168

Sugimoto, T. Zhou, X. & Muramatsu, A. (2003). Synthesis of uniform anatase TiO$_2$ nanoparticles by gel–sol method 4. Shape control. *J. Colloid Interface Sci.*, 259, pp. 53-61

Tang, Z. Kotov, N. A. & Giersig. M. (2002). Spontaneous Organization of single CdTe nanoparticles into luminescent nanowires. *Science*, 297, pp. 237-240

Tang, Z. Ozturk, B. Wang, Y. & Kotov. N. A. (2004). Simple preparation strategy and one-dimensional energy transfer in CdTe nanoparticle chains. *J. Phys. Chem. B*, 108, pp. 6927-6931

Wu, G. Zhang, L. Cheng, B. Xie, T. & Yuan, X. (2004). Synthesis of Eu$_2$O$_3$ nanotube arrays through a facile sol-gel template approach. *J. Am. Chem. Soc.*, 126, pp. 5976-5977

Yang, D. Wang, R. Zhang, J. & Liu, Z. (2004). Synthesis of nickel hydroxide nanoribbons with a new phase: A solution chemistry approach. *J. Phys. Chem. B*, 108, pp. 7531-7533

Yoshida, K. Jiu, J. Nagamatsu, D. Nemoto, T. Kurata, H. Adachi, M. & Isoda, S. (2008). Structure of TiO2 Nanorods formed with doiuble surfactants, *Molecular crystals and liquid crystals.* 491, pp. 14-20

Yu, W. W. Wang, Y. A. & Peng, X. (2003). Formation and stability of size-, shape-, and structure-controlled cdte nanocrystals: Ligand effects on monomers and nanocrystals. *Chem. Mater.*, 15, pp. 4300-4308

Zhang, H. Sun, J. Ma, D. Bao, X. Klein-Hoffmann, A. Weinberg, G. Su, D. & Schlogl, R. (2004). Unusual mesoporous SBA-15 with Parallel channels running along the short axis. *J. Am. Chem. Soc.*, 126, pp. 7440-7441

**Solar Cells - Dye-Sensitized Devices**

Edited by Prof. Leonid A. Kosyachenko

ISBN 978-953-307-735-2

Hard cover, 492 pages

**Publisher** InTech

**Published online** 09, November, 2011

**Published in print edition** November, 2011

The second book of the four-volume edition of "Solar cells" is devoted to dye-sensitized solar cells (DSSCs), which are considered to be extremely promising because they are made of low-cost materials with simple inexpensive manufacturing procedures and can be engineered into flexible sheets. DSSCs are emerged as a truly new class of energy conversion devices, which are representatives of the third generation solar technology. Mechanism of conversion of solar energy into electricity in these devices is quite peculiar. The achieved energy conversion efficiency in DSSCs is low, however, it has improved quickly in the last years. It is believed that DSSCs are still at the start of their development stage and will take a worthy place in the large-scale production for the future.

**How to reference**

In order to correctly reference this scholarly work, feel free to copy and paste the following:

Motonari Adachi, Katsuya Yoshida, Takehiro Kurata, Jun Adachi, Katsumi Tsuchiya, Yasushige Mori and Fumio Uchida (2011). Shape Control of Highly Crystallized Titania Nanorods for Dye-Sensitized Solar Cells Based on Formation Mechanism, Solar Cells - Dye-Sensitized Devices, Prof. Leonid A. Kosyachenko (Ed.), ISBN: 978-953-307-735-2, InTech, Available from: http://www.intechopen.com/books/solar-cells-dye-sensitized-devices/shape-control-of-highly-crystallized-titania-nanorods-for-dye-sensitized-solar-cells-based-on-format

# INTECH

open science | open minds